Hexagonal-shaped monolayer-bilayer quantum disks in graphene: A tight-binding approach

D. R. da Costa,[1,2,*] M. Zarenia,[2,†] Andrey Chaves,[1,3,‡] J. M. Pereira, Jr.,[1,§] G. A. Farias,[1,¶] and F. M. Peeters[2,1,**]

[1]*Departamento de Física, Universidade Federal do Ceará, 60455-900 Fortaleza, Ceará, Brazil*

[2]*Department of Physics, University of Antwerp, Groenenborgerlaan 171, B-2020 Antwerp, Belgium*

[3]*Department of Chemistry, Columbia University, 3000 Broadway, New York, New York 10027, USA*

(Received 4 May 2016; revised manuscript received 30 June 2016; published 11 July 2016)

Using the tight-binding approach, we investigate confined states in two different hybrid monolayer-bilayer systems: (i) a hexagonal monolayer area surrounded by bilayer graphene in the presence of a perpendicularly applied electric field and (ii) a hexagonal bilayer graphene dot surrounded by monolayer graphene. The dependence of the energy levels on dot size and external magnetic field is calculated. We find that the energy spectrum for quantum dots with zigzag edges consists of states inside the gap which range from dot-localized states, edge states, to mixed states coexisting together, whereas for dots with armchair edges, only dot-localized states are observed.

DOI: 10.1103/PhysRevB.94.035415

I. INTRODUCTION

Quantum dots (QDs) in monolayer [1,2] and bilayer [3–5] graphene have been the subject of a considerable number of both theoretical and experimental studies. Such QDs are expected to benefit from the exceptional properties of graphene, such as high carrier mobility and long spin coherence time for electronic and spintronic applications. However, the absence of an electronic band gap in both monolayer (MLG) and bilayer graphene (BLG) spectrum is the main obstacle preventing straightforward fabrication of graphene QDs, using electrostatic potential [6]. Nevertheless, in the case of BLG, it is known that a perpendicular electric field realized by external gate potentials applied to the different layers can open an energy gap [7]. Recent theoretical [8–11] and experimental [12,13] studies demonstrate electron confinement in gate-defined QDs created by tailoring the gap in BLG.

QDs in MLG have been fabricated by direct etching of pristine graphene sheets into small flakes. In these structures, the shape and edges of the sample can strongly influence the confined states. The electronic and transport properties of such QDs with different shapes and different edges have been investigated extensively [14–21]. Some theoretical studies have considered BLG flakes in which, in contrast to gate-defined QDs in BLG, edge disorder can also influence the electronic properties of the dot significantly [22–25]. For instance, the unbiased spectrum of AB-stacked BLG QDs with zigzag edges exhibits the well-known edge states, with a $2(N-1)$ fold-degenerate zero-energy level and a bunch of zero-energy states for the triangular and hexagonal QDs, respectively. In the presence of an electrostatic potential, the energy levels of BLG QDs with zigzag edges exhibit unusual states inside the gap, which correspond to the confinement at the edges: for hexagonal dots, these states are localized at the noninterlayer-connected zigzag edges and oscillate as either the dot size or the bias potential (V_0) increases, whereas for triangular dots, these states stem from the $E = V_0$ level that penetrates into the gap and resemble the nodal eigenstates of a quantum well along the zigzag edges of the system [24]. Under the influence of both electrostatic and a perpendicular magnetic field, the energy levels present different regions in the spectrum with respect to the crossing point between the lowest electron and hole Landau levels (LLs) of a biased BLG sheet that correspond to electron states localized at the center, edge, or corner of the BLG QD. For circular QDs, quantum Hall corner states are found to be absent, since those states appear only for geometries with corners. In contrast to the hexagonal BLG QDs, the energy spectrum of zigzag triangular BLG QDs do not preserve the electron-hole symmetry in the presence of an external gate potential [25].

Few layer graphene samples extracted from graphite are often found to contain patches of both MLG and BLG. Measurements have demonstrated the importance of monolayer-bilayer interface states for the transport and electronic properties of quantum structures based on such samples [26–31]. Monolayer-bilayer interface states have been theoretically investigated for a system of two semi-infinite MLG and BLG sheets with both zigzag- and armchair-terminated junctions in the absence [32,33] and presence [34,35] of an external magnetic field.

The existence of both monolayer and bilayer islands in exfoliated graphene samples motivated us to propose hybrid graphene QDs consisting of both MLG and BLG. In this paper, we study the confined states of the two different systems schematically depicted in Fig. 1: (a),(c) a hexagonal MLG dot surrounded by a hexagonal biased BLG region and (b),(d) a hexagonal BLG dot surrounded by a hexagonal region of MLG. The outer boundaries of the systems are assumed to be terminated by armchair (ac) edges, in order to avoid the influence of edge states corresponding to the outer hexagonal dot. For large enough samples, the QD states obtained are therefore not significantly influenced by the finite size of the total system and can be considered to be representative of an infinite system. Using the nearest-neighbor tight-binding formalism, we obtain the energy levels of these QDs for

*diego_rabelo@fisica.ufc.br
†mohammad.zarenia@uantwerpen.be
‡andrey@fisica.ufc.br
§pereira@fisica.ufc.br
¶gil@fisica.ufc.br
**francois.peeters@uantwerpen.be

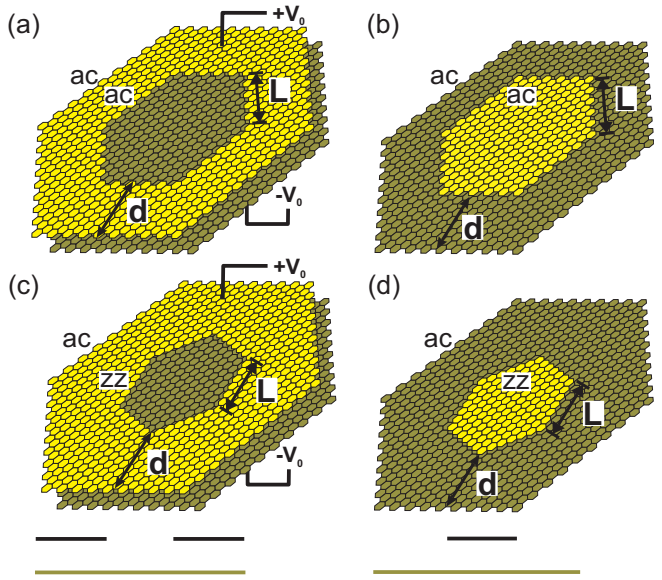

FIG. 1. Sketches of the studied systems, composed by hexagonal shaped QDs of side length L in BLG created by (a),(c) cutting out atoms in the inner region of the top layer and (b),(d) with the top layer being smaller than the bottom one. In both cases, the outer edges are taken as armchair forming a large size hexagonal dot and the inner edges are (a),(b) armchair and (c),(d) zigzag, respectively. Cross-sectional views of the dots are presented at the bottom of each system. We took $d \approx 10$ nm, which is sufficient for having confined states not affected by the finite size of the outer layer.

both zigzag (zz) and armchair terminated monolayer-bilayer interface. The results are obtained in both the absence and presence of a perpendicular magnetic field.

The paper is organized as follows. In Sec. II, we briefly discuss the tight-binding approach used in our numerical calculations. In Secs. IIIA and IIIB, we present our results for the energy levels of the QDs illustrated in Figs. 1(a),1(c) and 1(b),1(d), respectively, at zero magnetic field. In Secs. IVA and IVB, we investigate the influence of an external magnetic field on the electronic spectra of the proposed systems sketched in Figs. 1(a),1(c) and 1(b),1(d), respectively. Finally, we present our concluding remarks in Sec. V.

II. NUMERICAL METHOD

In order to describe electrons in AB-stacked BLG, we apply the tight-binding approximation, with the nearest-neighbor Hamiltonian,

$$H = \sum_{i \neq j} (\tau_{ij} c_i^\dagger c_j + \text{H.c.}) + \sum_i (\epsilon_i + V_i) c_i^\dagger c_i, \qquad (1)$$

where $\tau_{ij} = t = -2.7$ eV ($\tau_{ij} = t_\perp = 0.4$ eV) is the intra(inter)layer hopping energy term, the c_i ($c_i^\dagger$) operators annihilate (create) an electron at site i, and ϵ_i is the on-site energy. We included only the most significant interlayer hopping term, which is between the dimer sublattices A and B, i.e., between the atoms located directly on top of each other. The other interlayer hopping parameters γ_3 and γ_4 describe interlayer skew couplings between nondimer atoms A and B, and between dimer and nondimer atoms A and A or B and B, respectively. A tight-binding description for bilayer graphene considering only the perpendicular interlayer hopping yields a quadratic and isotropic energy dispersion that is valid near the Dirac points ($|E| \leqslant t_\perp$). At high energies and momentum far from the K point, trigonal warping effect and electron-hole asymmetry are observed. These influences in the energy spectrum are produced by the nonstrictly vertical hopping parameters γ_3 and γ_4, respectively [7,36–38]. From experimental papers reported in the literature, the parameter values, that fit the band structure predicted by the tight-binding model, have been obtained by comparison with observations from photoemission [39], Raman [40,41], and infrared spectroscopy [42–46]. The fitting tight-binding parameters in the vicinity of the corners of the Brillouin zone, that are commonly used in theoretical works, are given by $\gamma_3 \approx 0.3$ eV and $\gamma_4 \approx 0.14$ eV. Hence we neglect the influence of those second-nearest-neighbor parameters γ_3 and γ_4 that describe the nonorthogonality of adjacent atoms, since they have a small influence at low energy $|E| \leqslant t_\perp$ and are prevalent just near the Γ point at the center of the Brillouin zone. The on-site potential V_i is included only for the systems shown in Figs. 1(a) and 1(c), where we considered $V_i = -V_0$ and $V_i = V_0$ for the bottom and top layers, respectively, which induces a gap in the electronic spectrum. The tight-binding approach for BLG has been discussed [7,38,47] and successfully used [22–24,48] in many previous works in the literature, as well as in the theoretical treatment of the interface between MLG and BLG [32,35].

III. ZERO MAGNETIC FIELD

Let us first investigate the energy spectrum for zero magnetic field. In both cases, we show the dependence of the energy levels on the type of edge of the inner dot, i.e., zigzag or armchair.

A. Bilayer antidot

Figure 2 shows the energy spectrum as function of the antidot length L for hexagonal BLG QDs with armchair edges as sketched in Fig. 1(a). The potential $-V_0$ ($+V_0$) with $V_0 = 0.1$ eV is applied to the bottom (top) layer such that it opens a gap in the spectrum, as shown in Fig. 2(a). The spectrum exhibits an increasing number of energy levels inside the gap that are decreasing as function of the antidot length L. These energy levels correspond to states that are confined inside the monolayer. Outside the gap, the spectrum is continuous in the limit of an infinite bilayer system, i.e., $d \to \infty$. The total probability density function for the states indicated by points 1 and 2 in Fig. 2(a) are strongly localized (red color) around the center of the dot, i.e., monolayer region, as shown in Fig. 2(b), and the number of nodes increases for higher energy levels, as for conventional semiconductor quantum dot states. The reason for the states inside the gap is linked to the interplay between the electrostatic and structural confinements. The energy levels above ($E > V_0$) and below ($E < -V_0$) are spread out over the BLG region. There is a transition between dot-localized states that are found inside the gap ($|E| \lesssim V_0$) and states for which the probability density is spread along the outer hexagonal bilayer dot ($|E| > V_0$). These

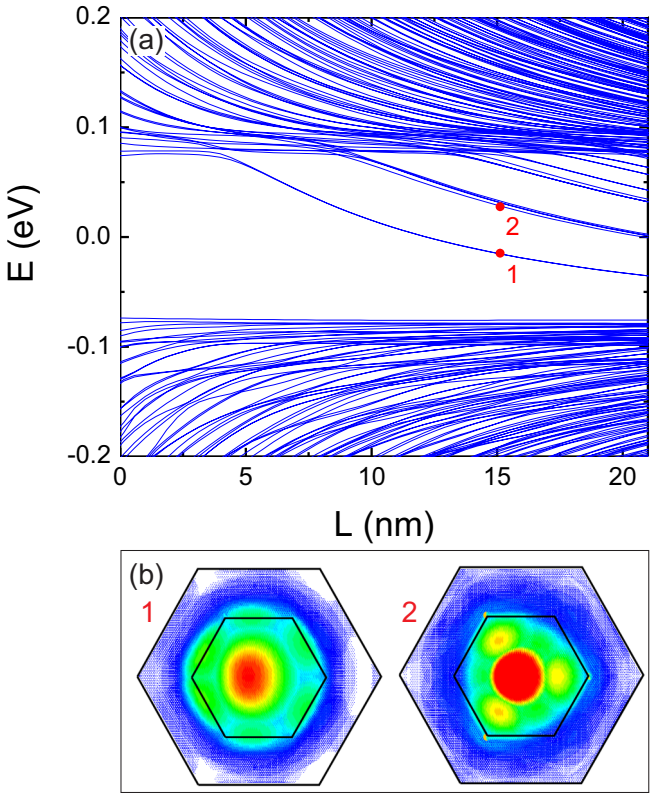

FIG. 2. (a) Energy spectrum of hexagonal MLG-BLG hybrid QDs with armchair edges as a function of dot side length L in the presence of electrical bias with $V_0 = 0.1$ eV for the system represented in Fig. 1(a). (b) Total probability density for the states labeled by 1 and 2 in (a). Blue (red) color represents low (high) density.

energy levels can be seen immediately below $E \approx V_0$ and above $E \approx -V_0$. They are almost independent of L and their probability densities (not shown here) exhibit confinement in both monolayer and bilayer regions. The fact that the opened gap in the spectrum of Fig. 2(a) is not exactly equal to $2V_0$ can be linked to the mexican-hat shape of the band structure of biased BLG, where the actual value of the band gap is not $2V_0$, since the minimum separation between the bands is not exactly at the K/K' points, but occurs at nonzero value of momentum away from the K/K' points [7,38].

The energy spectrum as a function of the antidot length L for hexagonal MLG-BLG hybrid QDs with zigzag edges is shown in Fig. 3. In the quest to obtain an energy spectrum with dot-localized states, as in the armchair case, a gate potential $-V_0$ $(+V_0)$ with $V_0 = 0.1$ eV is applied to the bottom (top) layer. In fact, due to the presence of zigzag edges, we obtain much more energy levels inside the gap, as compared to the armchair case. This is a characteristic signature of the zero energy states observed in monolayer graphene QDs with zigzag edges [14,49]. Note that if one superimposes the results of Fig. 2(a) on the spectrum of Fig. 3, it is seen that the anticrossing regions inside the gap of Fig. 3 match to a very good agreement. The additional states observed in Fig. 3 for hybrid MLG-BLG antidot with zigzag edges as compared to the armchair spectrum Fig. 2(a) suggest an interesting usage as a convenient tool for identifying zigzag and armchair samples

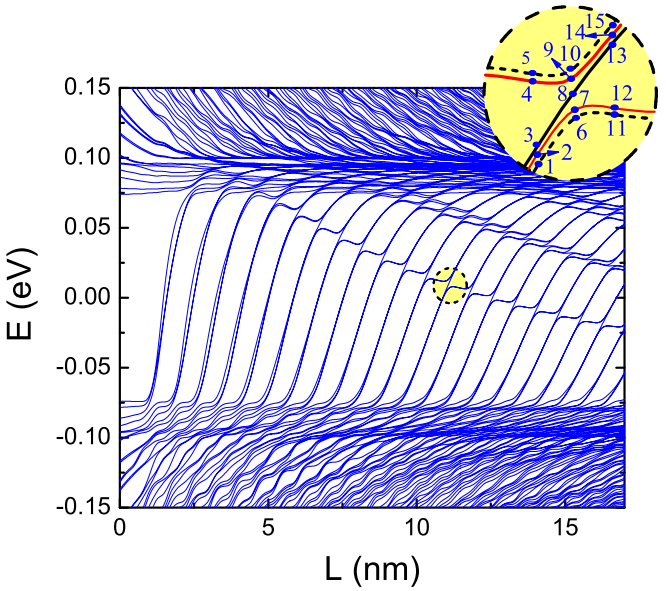

FIG. 3. Energy spectrum of hexagonal MLG-BLG hybrid QDs with zigzag edges as a function of dot side length L in the presence of a symmetric electrical bias with $V_0 = 0.1$ eV for the system represented in Fig. 1(c). An enlargement of the yellow region is shown to emphasize the behavior around the anticrossing of different states.

with similar geometric sizes, since those results have shown that the zigzag antidots possess a larger number of states inside the gap than for the armchair case. Another important remark about Fig. 3 is related to the anticrossings that appear in the spectrum, as shown in the enlarged region (yellow circle) around $L \approx 11$ nm. The corresponding electron probability densities for the points labeled by 1 to 15 in the enlarged circle are shown in Fig. 4, which demonstrate the following. (i) The almost threefold degenerate levels with increasing energy indicated by points 1, 2, and 3 correspond to states that are confined at the zigzag edges near the MLG-BLG junction [see Fig. 4(a)]. Even though the bottom layer does not present explicit edges close to the middle of the system, the electron can nevertheless be influenced by the upper layer edges due to the interlayer coupling near the MLG-BLG junction. (ii) The levels corresponding to states 4, 5, 11, and 12 are states localized inside the dot and their energies decrease as the antidot size increases [see Fig. 4(b)]. (iii) At the anticrossing (points 6, 7, 9 and 10) the electrons are confined due to the interplay between edge states corresponding to the zigzag edges and inside the dot owing to bias voltages, as presented in Fig. 4(c). (iv) The same kind of confinement as in points 1–3 was observed for the points 8–13 and 14,15 as shown in Figs. 4(d) and 4(e), respectively. Each set of points, formed by (a) 1, 2, and 3, and (d) 8 and 13, have the same symmetry and all of them are edge states whose only difference is the fact that they are rotated by $\pi/3$ due to the C_3 symmetry brought by the hexagonal geometry.

B. Bilayer quantum dot

Here, we study the dependence of the energy levels of the system sketched in Figs. 1(b) and 1(d), i.e., a hexagonal BLG QD surrounded by MLG, as a function of the BLG flake of

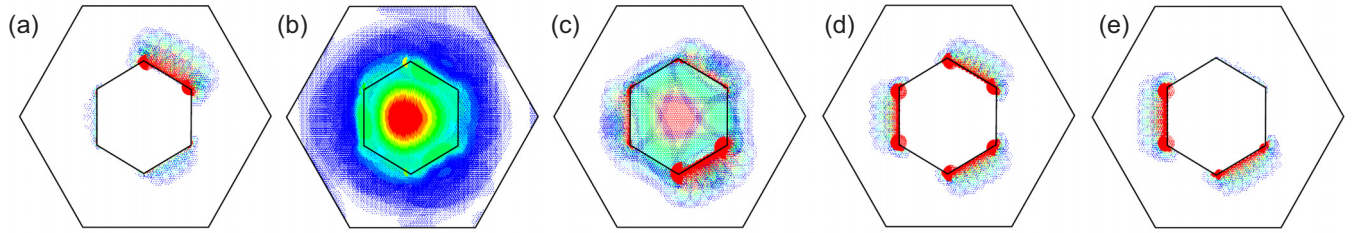

FIG. 4. Total probability density for the states labeled in Fig. 3 by (a) 1, 2, 3, (b) 4, 5, 11, 12, (c) 6, 7, 9, 10, (d) 8, 13, and (e) 14, 15. The wave functions corresponding to the states represented in the same panel have the same symmetry, but differ by a rotation with respect to each other and are therefore not shown. Blue (red) color represents low (high) density.

length L with BLG QD edges being (b) armchair and (d) zigzag, respectively. This analysis is done in the absence of any external potential, since for this case an applied electric field is not needed to confine carriers.

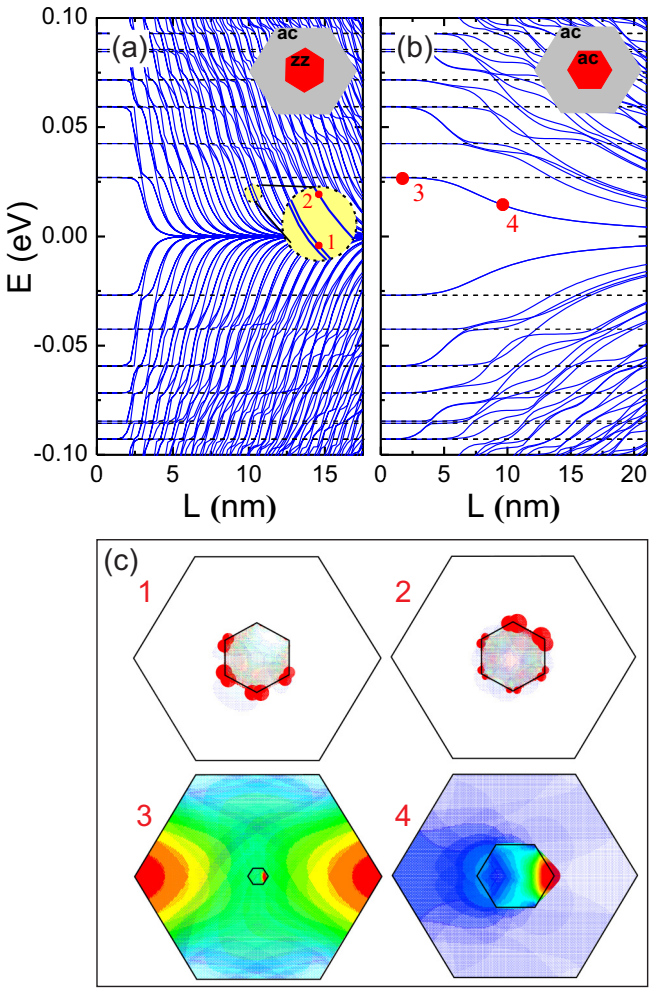

FIG. 5. Energy spectrum of hexagonal BLG QDs surrounded by a MLG flake with (a) zigzag and (b) armchair edges as a function of dot side length L for the system represented in Figs. 1(d) and 1(b), respectively. The dashed black lines are the energy levels of the monolayer system that has the same dimension as the bottom layer for the bilayer system sketched in Figs. 1(b) and 1(d). (c) The corresponding total probability density for the states labeled by 1 and 2 in (a) for the zigzag case and 3 and 4 in (b) for the armchair case. Blue (red) color represents low (high) density.

A general feature of this kind of system is that the energy spectrum for QDs formed by both zigzag and armchair edges, shown in Figs. 5(a) and 5(b), respectively, does not change for sizes $L \lesssim 2.5$ nm ($L \lesssim 4$ nm) for the zigzag (armchair) case. This is due to the fact that for small sizes of the BLG dot, the energy spectrum forms plateaus converging to the energy levels of the outer hexagonal MLG QD with armchair edges [see the black dashed lines in Figs. 5(a) and 5(b)]. These levels are independent of the edges at the MLG-BLG junction. As the size of the BLG QD increases, the degeneracy of the energy levels is lifted and the plateaus become less pronounced. For both edge terminations, the energy levels decrease as L increases, though differing in two aspects: (i) for the zigzag case, more confined states are observed and their energies decrease with L, converging to zero energy and forming plateaus at energies that match the MLG energy levels and (ii) the energy gap in the armchair spectrum stays open even for large dot sizes. In Fig. 5(c), we show the total probability density for the points 1,2 and 3,4 labeled in Figs. 5(a) and 5(b), respectively. As shown in the zoomed circle in Fig. 5(a) around $L \approx 10$ nm, three states that are decreasing in energy, two of them being approximately degenerate ($E \approx 0.02150$ eV and $E \approx 0.02159$ eV). It was verified that these two states arise from the same initial plateau; hence their wave functions display the same behavior and symmetry, as shown in panel 1 of Fig. 5(c). Both levels are essentially edge states and only differ by a rotation of π. The other energy level, panel 2 in Fig. 5(c), with energy $E \approx 0.02556$ eV, is a combination of two edge states, as in panel 1, and a less pronounced center-localized state. The probability densities for the ground state of the armchair spectrum are shown in panels 3 and 4 of Fig. 5(c). Point 3 corresponds to the first plateau with $L \approx 2.272$ nm and, since the BLG region is much smaller than the single layer region, the total probability density approaches the ground state for a hexagonal MLG QD [18]. This state is clearly not a QD state of the proposed BLG system, being just a consequence of the finite size of the simulated system. On the other hand, for large dot size, e.g., $L \approx 9.94$ nm (point 4), one finds a dot-localized state, with $|\psi|^2$ confined in the BLG area.

IV. MAGNETIC FIELD EFFECT

In this section, we investigate the influence of an external magnetic field, with possible addition or not of a bias voltage for the system sketched in Figs. 1(a) and 1(c) and the unbiased case for the system illustrated in Figs. 1(b) and 1(d).

The effect of an external magnetic field is incorporated in the tight-binding model via the Peierls substitution, i.e., a phase is included in the intralayer hopping parameters, such that $\tau_{ij} \rightarrow \tau_{ij} \exp[i\frac{e}{\hbar}\int_j^i \vec{A}\cdot d\vec{l}]$, where $\vec{A}$ is the vector potential that corresponds to the applied magnetic field. We choose the Landau gauge $\vec{A} = (0, Bx, 0)$, for a magnetic field perpendicular to the plane of the sample $\vec{B} = B\hat{z}$. For the chosen gauge, the Peierls phase becomes zero and $\exp[\frac{2\pi i x\phi}{3a\phi_0}]$ in the x and y directions, respectively, where $a = 0.142$ nm is the lattice parameter of graphene, $\phi_0 = h/e$ is the quantum of magnetic flux, and $\phi = 3\sqrt{3}a^2B/2$ is the magnetic flux through one carbon hexagon. The magnetic field has no effect on the interlayer hopping $t_\perp$. In this section, the results for the zigzag and armchair edges are obtained for antidots [the system shown in Figs. 1(a) and 1(c)] and dots [the system shown in Figs. 1(b) and 1(d)] with sides, respectively $L \approx 4.919$ nm and $L \approx 5.254$ nm, corresponding to $N = 20$ and $N = 13$ hexagonal carbon rings on each side.

A. Bilayer antidot

In Fig. 6 we show the results for the unbiased energy spectrum of hexagonal MLG-BLG hybrid QDs with (a) armchair and (b) zigzag edges as a function of the magnetic flux (ϕ/ϕ_0). In general, for both edge terminations, as the magnetic flux increases, the energy levels approach the Landau levels (LLs) of an unbiased BLG sheet [11,50], shown by the red dashed lines. The results show that the energy spectrum exhibits electron-hole symmetry, i.e., $E_h = -E_e$, where $h(e)$ index denotes hole (electron). Comparing Figs. 6(a) and 6(b), one notices that the energy levels are similar, except for the low energy limit where (i) the spectrum for zigzag QD exhibits a number of states near zero energy that correspond to edge states, not present in armchair QDs, whereas (ii) the spectrum for armchair QD exhibits a small gap around $E = 0$, as shown by the insets in Figs. 6(a) and 6(b). As the magnetic flux increases, the degeneracy of the energy levels is lifted, resulting in a closing of the energy gap in the spectrum of armchair QD. These two features are reminiscent of the energy spectra of zigzag and armchair QDs in MLG under the influence of an external magnetic field (see Refs. [17], [49], and [51]). The interplay between confinement by the magnetic field and QD-localized states leads to the appearance of several branch crossings and anticrossings for both zigzag and armchair cases, as shown by the magnification in Fig. 6(a). They consist of two groups of states: (i) the levels decreasing with magnetic flux, which correspond to the quantum Hall edge states confined at the edges of the outer armchair hexagonal dot (consequently, these states are not QD states) and (ii) the quantum Hall edge states pertinent to the confinement at the MLG-BLG junction. This is verified in Fig. 6(c), where the total electron density for the states labeled as 1 [chosen from group (i)] and 2 [chosen from group (ii)] are shown. This way we can state that the presence of the branches that increase (decrease) in energy as shown in the inset of Fig. 6(a) can be attributed to the existence of quantum Hall edge states along the external (internal) edges. In a semiclassical view, these edge states correspond to skipping orbits that lead, for the external edge, to a current that generates a magnetic moment parallel to the magnetic field, whereas for the internal edge the magnetic moment opposes the external field.

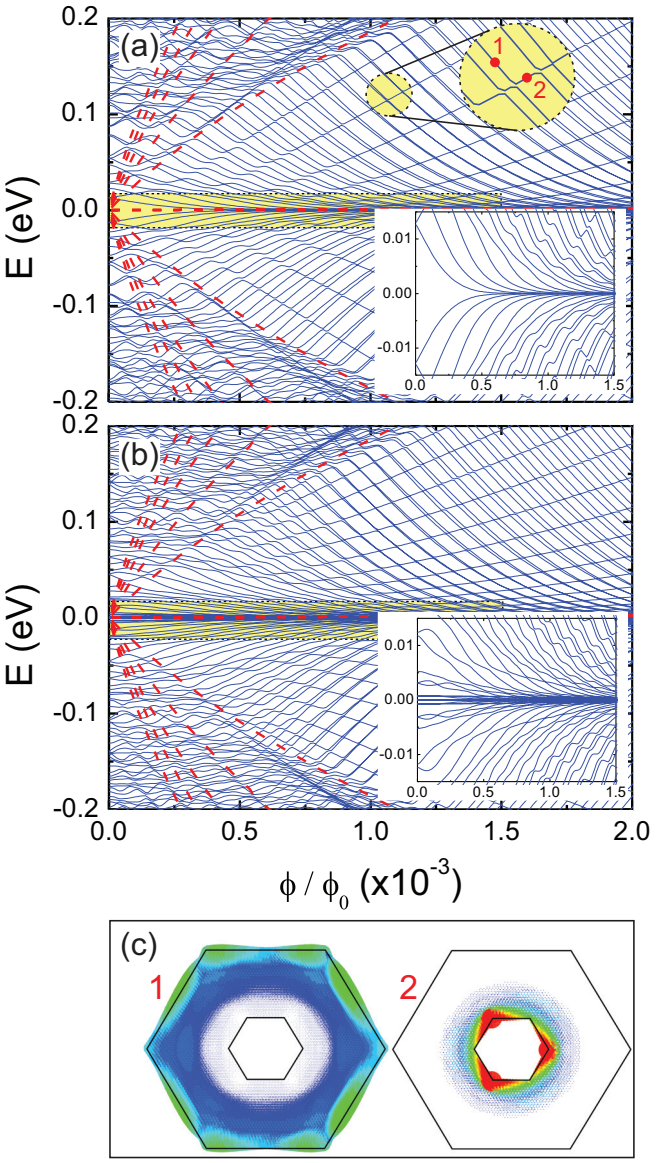

FIG. 6. Energy spectrum of hexagonal MLG-BLG hybrid QDs with (a) armchair and (b) zigzag edges as a function of magnetic flux in the absence of electrical bias for the system represented in Figs. 1(a) and 1(c). The red dashed curves correspond to the LLs of an unbiased infinite BLG. The insets in (a) and (b) show a zoom around $E = 0$. (c) The total probability density for the states corresponding to the points labeled by 1 and 2 in (a). Blue (red) color represents low (high) density.

Figures 7 and 8 display the effect of a bias potential ($V_0 = 0.1$ eV) on the magnetic spectra of hexagonal MLG-BLG hybrid QDs for antidots with armchair and zigzag edges, respectively. The energy spectra for both edge terminations approach the LLs of an infinite biased BLG sheet, shown by the red dashed curves [50,52,53]. A striking feature of these results is that the energy levels have a nonmonotonic dependence on the magnetic field, which is not found for the unbiased case. The lowest electron and hole LLs are found to intersect at $E = 0$. As discussed in Refs. [50] and [25],

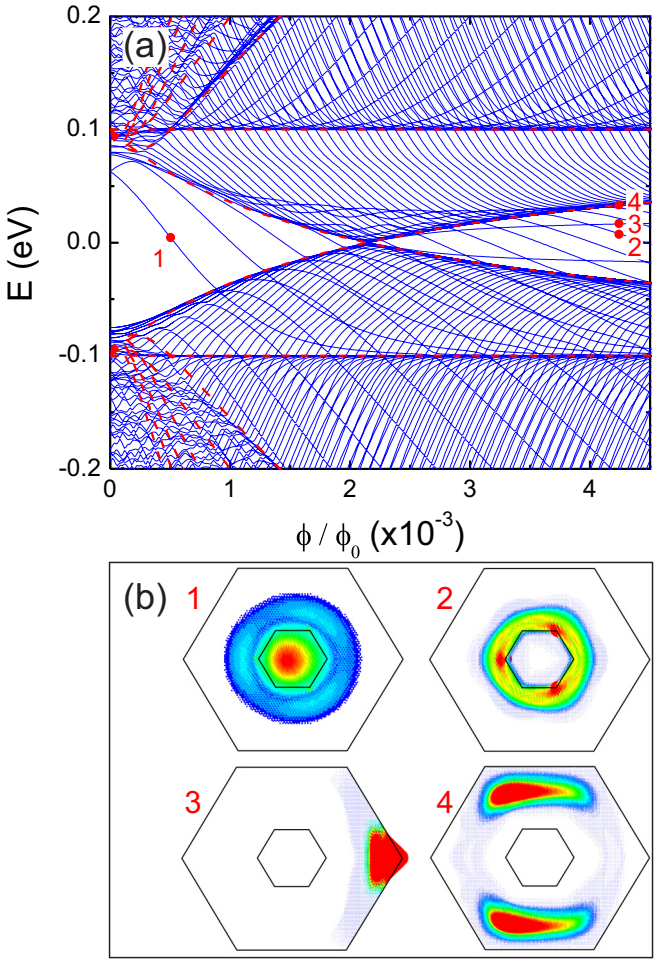

FIG. 7. (a) Energy spectrum of hexagonal MLG-BLG hybrid QDs for the antidot with armchair edges as a function of magnetic flux in the presence of electrical bias with $V_0 = 0.1$ eV for the system represented in Fig. 1(a). The red dashed curves correspond to the LLs of an infinite biased BLG. (b) The total probability density for the points labeled by 1–4 in (a). Blue (red) color represents low (high) density.

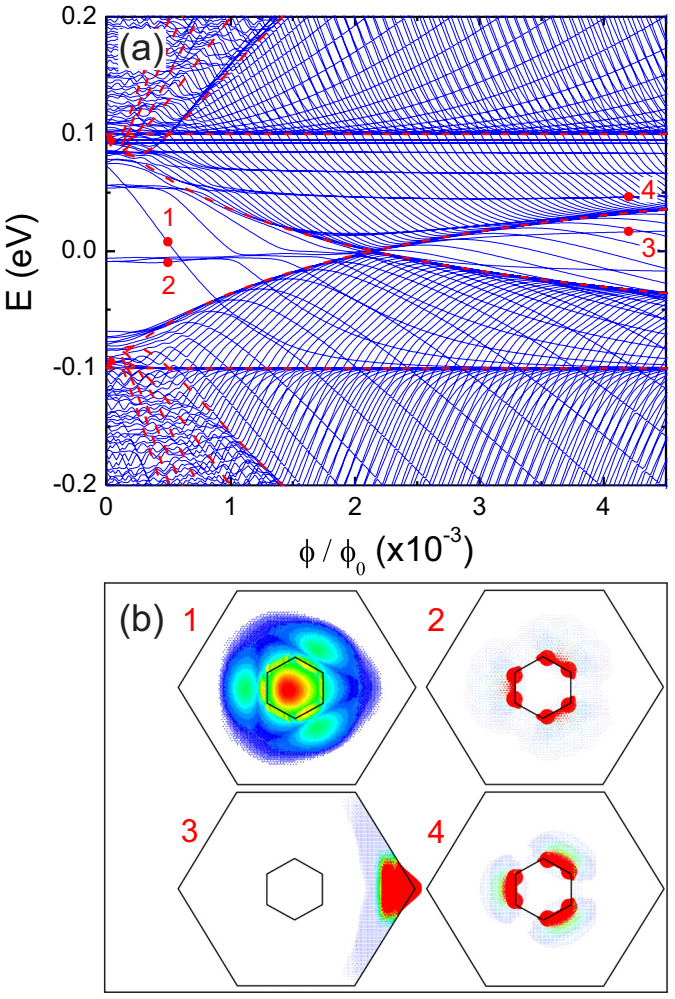

FIG. 8. Same as in Fig. 7, but now for hexagonal MLG-BLG hybrid QDs with zigzag antidot edges [as sketched in Fig. 1(c)].

the crossings between the two lowest LLs for a biased BLG occur at larger values of the magnetic field as the bias increases. One important consequence of the presence of a magnetic field together with the electrostatic confinement is the breaking of inversion symmetry, i.e., the spectrum is no longer electron-hole symmetric ($E_h \neq -E_e$). For small values of ϕ/ϕ_0, the spectra for both edge terminations exhibit a large gap around $E = 0$. Similar to the decreasing levels inside the gap in Figs. 2(a) and 3, the states inside the energy gap range, at fields lower than that where the crossing between the two lowest zeroth biased LLs occurs, exhibit the same feature: a centered-peak localized state, as the one shown in panel 1 of Figs. 7(b) and 8(b), respectively for antidots with armchair and zigzag inner edges. In addition to the QD confined states, the zigzag spectrum in Fig. 8(a) shows subbands of energies composed by three states, which are weakly dependent on the magnetic field. These energy levels are edge states as shown in panel 2 of Fig. 8(b), and they have the same symmetry, albeit rotated by a phase of $\pi/3$ from each other, respecting the C_3 symmetry. Similar behavior is observed also for the same states in the positive part of the zigzag biased QD spectrum. The total probability density of one of these states is shown in panel 4 of Fig. 8(b) and presents confinement at the QD edges, just like the one in panel 2 in Fig. 8(b). For higher magnetic flux, away from the crossing point between the two lowest biased LLs, two groups of states are found: pure corner states [see panels 3 in Figs. 7(b) and 8(b)] and states confined along the antidot boundaries [see panels 2 in Fig. 7(b)]. In our recent work [25], we investigated similar corner states and found that they are absent in circular BLG QDs. For the states with higher energy, more peaks are observed in the delocalized probability density, as shown in panel 4 of Fig. 7(b) for one of the states composing the upper zeroth LL, whose probability density exhibits two peaks in the monolayer region of the system. States labeled by points 3 and 4 in Fig. 7(b) and by point 3 in Fig. 8(b) are not QD states, being just a consequence of the finite size of the simulated system.

B. Bilayer quantum dot

In this section, we investigate the influence of a perpendicular magnetic field on the energy levels of hexagonal

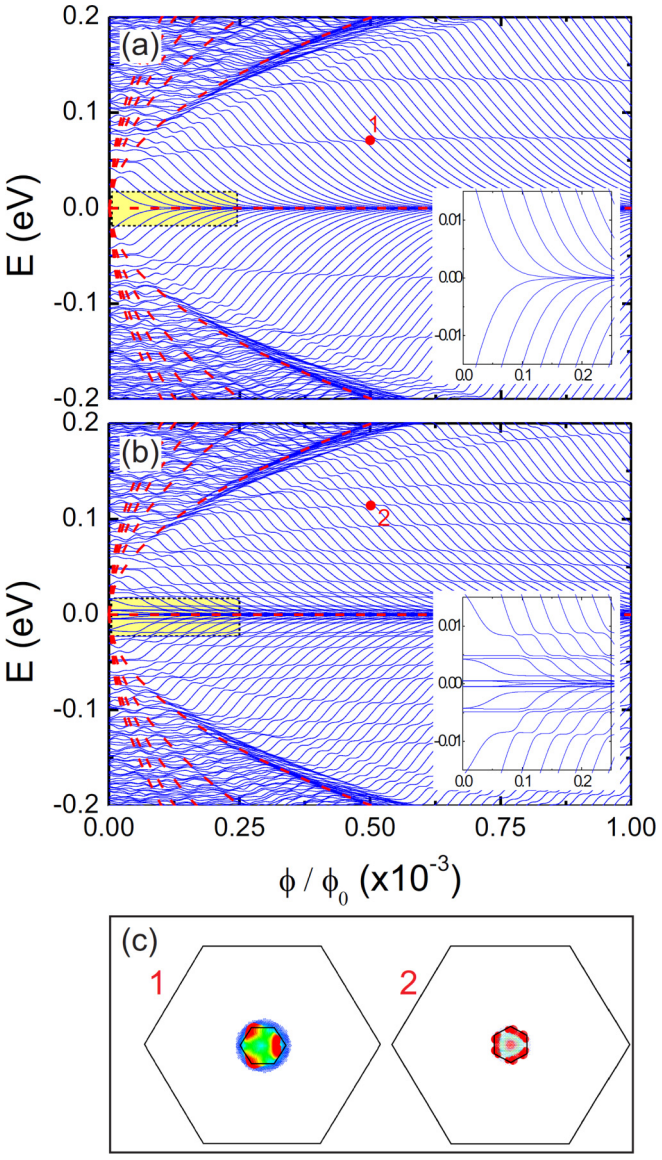

FIG. 9. Energy spectrum of hexagonal BLG QDs surrounded by a hexagonal MLG flake with (a) armchair and (b) zigzag edges as a function of magnetic flux in the absence of electrical bias for the systems represented in Figs. 1(d) and 1(b), respectively. The red dashed curves correspond to the LLs of an unbiased infinite MLG. The insets in (a) and (b) show a zoom around $E = 0$. (c) The total probability density for the points labeled by 1 and 2 in (a) and (b), respectively. Blue (red) color represents low (high) density.

BLG QDs surrounded by MLG [the systems are sketched in Figs. 1(b) and 1(d), respectively, for inner armchair and zigzag edges]. These results are shown in Figs. 9(a) and 9(b) for the unbiased case, assuming BLG QD edges as armchair and zigzag, respectively. As done in Sec. IIB, our study for the BLG dots is performed in the absence of any applied electric field, since no external potential is needed for this case in order to confine the charge carriers. It is important to point out that for the present case, the energy spectra for both edge terminations converge to LLs of an unbiased infinite MLG, whereas the results obtained for MLG-BLG hybrid QDs shown in the previous subsection (IVA) approach the unbiased BLG LLs. This is expected, since for large magnetic fields the effect of the MLG (BLG) region can be regarded as a small perturbation to the BLG (MLG) LL spectrum for the MLG-BLG antidot (BLG dot) case, due to the fact that the magnetic length in this case becomes smaller than the characteristic size of the MLG (BLG) region. In addition, although one may expect the situation to be the opposite, i.e., for the large magnetic field the energy spectra of the MLG-BLG antidots (BLG QDs surrounded by a MLG) should approach the MLG (BLG) LLs, one has to keep in mind that the larger outer systems are BLG (MLG) QDs, and the states that are following the LLs are those with very high energy, which in general are states whose total probability density spread along the whole system, and not only in the central region. Therefore, it makes sense that these states converge rather to LLs of the bilayer (monolayer). Some similarities as compared to the results obtained for the BLG antidots (shown in Fig. 6) can be observed: (i) the energy spectra exhibit electron-hole symmetry, (ii) for small magnetic flux the armchair spectrum presents a small gap around $E = 0$ [see inset in Fig. 9(a)], (iii) the zigzag spectrum has a bunch of zero energy states corresponding to edge states [see inset in Fig. 9(b)], and (iv) the states that decrease in energy are quantum Hall edge states along the external edges, i.e., they spread along the MLG edges for the present case. Note that the $E > 0$ electron states whose energy increase with magnetic flux and are below the first LL consist of pure QD-localized states for the armchair case and a mix of QD-localized states and quantum Hall edge states that is pertinent to the confinement at the MLG-BLG junction for the zigzag BLG QD. The total electron densities for these states are shown in Fig. 9(c) labeled by 1 and 2 for the armchair and zigzag BLG QDs, respectively.

V. CONCLUSIONS

We presented a theoretical study of the energy levels within the tight-binding approach for two different types of QD systems that are realized through MLG-BLG junctions. They consist of hexagonal BLG QDs created by (i) cutting out atoms in the inner region of the top layer, forming an hexagonal BLG antidot, or (ii) a hexagonal BLG QD at the top layer surrounded by a hexagonal region of MLG. We have numerically obtained the energy spectra for both QDs with armchair and zigzag edges and discussed localization of carriers in these hybrid MLG-BLG QDs, analyzing the energy spectra in the presence of an external magnetic field and a gate potential.

In the absence of magnetic field, we have demonstrated that the antidot BLG system exhibits localized states in MLG in the presence of bias potential. For the case of zigzag edges, we found additional states inside the gap region which increase with size and correspond to edge states. Another feature observed in this case is the appearance of anticrossings in the spectrum, related to the interplay between the zigzag edge states near the MLG-BLG junction and states inside the dot confined by the bias voltage.

In the presence of a perpendicular magnetic field for the case of BLG antidot, we found that the energy levels approach the BLG LLs for both edge terminations, whereas for the BLG QD surrounded by a MLG we observed that the energy spectra converge to the MLG LLs for large magnetic flux. Similar to

the hexagonal MLG QDs, we demonstrated that the energy spectrum as a function of the magnetic flux exhibits a gap for smaller values of magnetic flux in the armchair dot case and many additional zero energies making a bunch of edge states for the zigzag QD. Furthermore, the energy spectrum for the unbiased case exhibits (i) electron-hole symmetry and (ii) several crossing and anticrossings for both edge terminations that can be linked to the interplay between the magnetic field confinement and the QD confinement.

We found that the biased MLG-BLG hybrid QD spectra present regions with different regimes with respect to the intersection point between the lowest electron and hole LLs. We showed that those different regimes correspond to states confined at the center, the edge, and the corner of the BLG QD. Another important consequence of the combination of magnetic field and an electrostatic confinement is that it breaks the inversion symmetry of the bilayer system and consequently the electron-hole symmetry is not preserved in the energy spectrum.

The hybrid QDs proposed in this paper could be realized experimentally by employing block copolymer lithography [54–56] or by involving standard electron beam lithography [57–59] to etch the antidot pattern in the upper layer, and the control of the antidot edge termination can be realized by heat treatment [58] or selective etching [59]. Although we have shown the results for the hexagonal geometry, our paper presents a proof of concept that hybrid systems as the ones defined by MLG and BLG can in fact be used as quantum confined devices that manipulate electrons in graphene based nanostructures, and such are attractive candidates for nanoelectronics applications [12,29–31].

ACKNOWLEDGMENTS

This work was financially supported by CNPq, under contract NanoBioEstruturas No. 555183/2005-0, PRONEX/FUNCAP, CAPES Foundation, under the process No. BEX 7178/13-1, the Flemish Science Foundation (FWO-Vl), the Bilateral programme between CNPq and FWO-Vl, the Brazilian Program Science Without Borders (CsF), and the Lemann Foundation.

[1] K. S. Novoselov, A. K. Geim, S. V. Morozov, D. Jiang, Y. Zhang, S. V. Dubonos, I. V. Grigorieva, and A. A. Firsov, Electric field effect in atomically thin carbon films, Science **306**, 666 (2004).

[2] A. H. Castro Neto, F. Guinea, N. M. R. Peres, K. S. Novoselov, and A. K. Geim, The electronic properties of graphene, Rev. Mod. Phys. **81**, 109 (2009).

[3] A. V. Rozhkov, G. Giavaras, Y. P. Bliokh, V. Freilikher, and F. Nori, Electronic properties of mesoscopic graphene structures: Charge confinement and control of spin and charge transport, Phys. Rep. **503**, 77 (2011).

[4] W.-d. Sheng, M. Korkusinski, A. D. Güçlü, M. Zielinski, P. Potasz, E. S. Kadantsev, O. Voznyy, and P. Hawrylak, Electronic and optical properties of semiconductor and graphene quantum dots, Front. Phys. **7**, 328 (2012).

[5] F. Molitor, J. Güttinger, C. Stampfer, S. Dröscher, A. Jacobsen, T. Ihn, and K. Ensslin, Electronic properties of graphene nanostructures, J. Phys.: Condens. Matter **23**, 243201 (2011).

[6] C. A. Downing, A. R. Pearce, R. J. Churchill, and M. E. Portnoi, Optimal traps in graphene, Phys. Rev. B **92**, 165401 (2015).

[7] E. McCann and M. Koshino, The electronic properties of bilayer graphene, Rep. Prog. Phys. **76**, 056503 (2013).

[8] A. Matulis and F. M. Peeters, Quasibound states of quantum dots in single and bilayer graphene, Phys. Rev. B **77**, 115423 (2008).

[9] P. Recher, J. Nilsson, G. Burkard, and B. Trauzettel, Bound states and magnetic field induced valley splitting in gate-tunable graphene quantum dots, Phys. Rev. B **79**, 085407 (2009).

[10] J. M. Pereira, Jr., P. Vasilopoulos, and F. M. Peeters, Tunable quantum dots in bilayer graphene, Nano Lett. **7**, 946 (2007).

[11] J. M. Pereira, Jr., F. M. Peeters, P. Vasilopoulos, R. N. Costa Filho, and G. A. Farias, Landau levels in graphene bilayer quantum dots, Phys. Rev. B **79**, 195403 (2009).

[12] M. T. Allen, J. Martin, and A. Yacoby, Gate-defined quantum confinement in suspended bilayer graphene, Nat. Commun. **3**, 934 (2012).

[13] A. M. Goossens, S. C. M. Driessen, T. A. Baart, K. Watanabe, T. Taniguchi, and L. M. K. Vandersypen, Gate-defined confinement in bilayer graphene-hexagonal boron nitride hybrid devices, Nano Lett. **12**, 4656 (2012).

[14] D. R. da Costa, A. Chaves, M. Zarenia, J. M. Pereira, Jr., G. A. Farias, and F. M. Peeters, Geometry and edge effects on the energy levels of graphene quantum rings: A comparison between tight-binding and simplified Dirac models, Phys. Rev. B **89**, 075418 (2014).

[15] A. V. Rozhkov and F. Nori, Exact wave functions for an electron on a graphene triangular quantum dot, Phys. Rev. B **81**, 155401 (2010).

[16] M. Zarenia, J. M. Pereira, Jr., A. Chaves, F. M. Peeters, and G. A. Farias, Simplified model for the energy levels of quantum rings in single layer and bilayer graphene, Phys. Rev. B **81**, 045431 (2010).

[17] M. Grujić, M. Zarenia, A. Chaves, M. Tadić, G. A. Farias, and F. M. Peeters, Electronic and optical properties of a circular graphene quantum dot in a magnetic field: Influence of the boundary conditions, Phys. Rev. B **84**, 205441 (2011).

[18] M. Zarenia, A. Chaves, G. A. Farias, and F. M. Peeters, Energy levels of triangular and hexagonal graphene quantum dots: A comparative study between the tight-binding and Dirac equation approach, Phys. Rev. B **84**, 245403 (2011).

[19] H. P. Heiskanen, M. Manninen, and J. Akola, Electronic structure of triangular, hexagonal and round graphene flakes near the Fermi level, New J. Phys. **10**, 103015 (2008).

[20] M. Ezawa, Metallic graphene nanodisks: Electronic and magnetic properties, Phys. Rev. B **76**, 245415 (2007).

[21] S. Schnez, K. Ensslin, M. Sigrist, and T. Ihn, Analytic model of the energy spectrum of a graphene quantum dot in a perpendicular magnetic field, Phys. Rev. B **78**, 195427 (2008).

[22] A. D. Güçlü, P. Potasz, and P. Hawrylak, Electric-field controlled spin in bilayer triangular graphene quantum dots, Phys. Rev. B **84**, 035425 (2011).

[23] D. P. Zebrowski, E. Wach, and B. Szafran, Confined states in quantum dots defined within finite flakes of bilayer graphene: Coupling to the edge, ionization threshold, and valley degeneracy, Phys. Rev. B **88**, 165405 (2013).

[24] D. R. da Costa, M. Zarenia, A. Chaves, G. A. Farias, and F. M. Peeters, Energy levels of bilayer graphene quantum dots, Phys. Rev. B **92**, 115437 (2015).

[25] D. R. da Costa, M. Zarenia, A. Chaves, G. A. Farias, and F. M. Peeters, Magnetic field dependence of energy levels in biased bilayer graphene quantum dots, Phys. Rev. B **93**, 085401 (2016).

[26] Y. Kobayashi, K. I. Fukui, T. Enoki, K. Kusakabe, and Y. Kaburagi, Observation of zigzag and armchair edges of graphite using scanning tunneling microscopy and spectroscopy, Phys. Rev. B **71**, 193406 (2005).

[27] Y. Niimi, T. Matsui, H. Kambara, K. Tagami, M. Tsukada, and H. Fukuyama, Scanning tunneling microscopy and spectroscopy of the electronic local density of states of graphite surfaces near monoatomic step edges, Phys. Rev. B **73**, 085421 (2006).

[28] C. P. Puls, N. E. Staley, and Y. Liu, Interface states and anomalous quantum oscillations in hybrid graphene structures, Phys. Rev. B **79**, 235415 (2009).

[29] A. Iagallo, S. Tanabe, S. Roddaro, M. Takamura, Y. Sekine, H. Hibino, V. Miseikis, C. Coletti, V. Piazza, F. Beltram, and S. Heun, Bilayer-induced asymmetric quantum Hall effect in epitaxial graphene, Semicond. Sci. Technol. **30**, 055007 (2015).

[30] Y. Nam, J. Sun, N. Lindvall, S. J. Yang, D. Kireev, Ch. R. Park, Y. W. Park, and A. Yurgens, Quantum Hall effect in graphene decorated with disordered multilayer patches, Appl. Phys. Lett. **103**, 233110 (2013).

[31] F. Giannazzo, I. Deretzis, A. La Magna, F. Roccaforte, and R. Yakimova, Electronic transport at monolayer-bilayer junctions in epitaxial graphene on SiC, Phys. Rev. B **86**, 235422 (2012).

[32] E. V. Castro, N. M. R. Peres, and J. M. B. Lopes dos Santos, Localized states at zigzag edges of multilayer graphene and graphite steps, Europhys. Lett. **84**, 17001 (2008).

[33] T. Nakanishi, M. Koshino, and T. Ando, Transmission through a boundary between monolayer and bilayer graphene, Phys. Rev. B **82**, 125428 (2010).

[34] M. Koshino, T. Nakanishi, and T. Ando, Interface Landau levels in graphene monolayer-bilayer junctions, Phys. Rev. B **82**, 205436 (2010).

[35] Z.-x. Hu and W. Ding, Edge states at the interface between monolayer and bilayer graphene, Phys. Lett. A **376**, 610 (2012).

[36] E. McCann, D. S. L. Abergel, and V. I. Fal'ko, The low energy electronic band structure of bilayer graphene, Eur. Phys. J. Spec. Top. **148**, 91 (2007).

[37] E. McCann and V. I. Fal'ko, Landau-Level Degeneracy and Quantum Hall Effect in a Graphite Bilayer, Phys. Rev. Lett. **96**, 086805 (2006).

[38] E. McCann, D. S. L. Abergel, and V. I. Fal'ko, Electrons in bilayer graphene, Solid State Commun. **143**, 110 (2007).

[39] T. Ohta, A. Bostwick, T. Seyller, K. Horn, and E. Rotenberg, Controlling the electronic structure of bilayer graphene, Science **313**, 951 (2006).

[40] L. M. Malard, J. Nilsson, D. C. Elias, J. C. Brant, F. Plentz, E. S. Alves, A. H. Castro Neto, and M. A. Pimenta, Probing the electronic structure of bilayer graphene by Raman scattering, Phys. Rev. B **76**, 201401(R) (2007).

[41] A. Das, B. Chakraborty, S. Piscanec, S. Pisana, A. K. Sood, and A. C. Ferrari, Phonon renormalization in doped bilayer graphene, Phys. Rev. B **79**, 155417 (2009).

[42] L. M. Zhang, Z. Q. Li, D. N. Basov, M. M. Fogler, Z. Hao, and M. C. Martin, Determination of the electronic structure of bilayer graphene from infrared spectroscopy, Phys. Rev. B **78**, 235408 (2008).

[43] Z. Q. Li, E. A. Henriksen, Z. Jiang, Z. Hao, M. C. Martin, P. Kim, H. L. Stormer, and D. N. Basov, Band Structure Asymmetry of Bilayer Graphene Revealed by Infrared Spectroscopy, Phys. Rev. Lett. **102**, 037403 (2009).

[44] E. A. Henriksen, Z. Jiang, L.-C. Tung, M. E. Schwartz, M. Takita, Y.-J. Wang, P. Kim, and H. L. Stormer, Cyclotron Resonance in Bilayer Graphene, Phys. Rev. Lett. **100**, 087403 (2008).

[45] A. B. Kuzmenko, E. van Heumen, D. van der Marel, P. Lerch, P. Blake, K. S. Novoselov, and A. K. Geim, Infrared spectroscopy of electronic bands in bilayer graphene, Phys. Rev. B **79**, 115441 (2009).

[46] A. B. Kuzmenko, I. Crassee, D. van der Marel, P. Blake, and K. S. Novoselov, Determination of the gate-tunable band gap and tight-binding parameters in bilayer graphene using infrared spectroscopy, Phys. Rev. B **80**, 165406 (2009).

[47] E. V. Castro, N. M. R. Peres, J. M. B. Lopes dos Santos, A. H. Castro Neto, and F. Guinea, Localized States at Zigzag Edges of Bilayer Graphene, Phys. Rev. Lett. **100**, 026802 (2008).

[48] D. R. da Costa, M. Zarenia, A. Chaves, G. A. Farias, and F. M. Peeters, Analytical study of the energy levels in bilayer graphene quantum dots, Carbon **78**, 392 (2014).

[49] Z. Z. Zhang, K. Chang, and F. M. Peeters, Tuning of energy levels and optical properties of graphene quantum dots, Phys. Rev. B **77**, 235411 (2008).

[50] J. M. Pereira, Jr., F. M. Peeters, and P. Vasilopoulos, Landau levels and oscillator strength in a biased bilayer of graphene, Phys. Rev. B **76**, 115419 (2007).

[51] D. A. Bahamon, A. L. C. Pereira, and P. A. Schulz, Inner and outer edge states in graphene rings: A numerical investigation, Phys. Rev. B **79**, 125414 (2009).

[52] L. M. Zhang, M. M. Fogler, and D. P. Arovas, Magnetoelectric coupling, Berry phase, and Landau level dispersion in a biased bilayer graphene, Phys. Rev. B **84**, 075451 (2011).

[53] D. Wang and G. Jin, Combined effect of magnetic and electric fields on Landau level spectrum and magneto-optical absorption in bilayer graphene, Europhys. Lett. **92**, 57008 (2010).

[54] M. Kim, N. S. Safron, E. Han, M. S. Arnold, and P. Gopalan, Fabrication and characterization of large-area, semiconducting nanoperforated graphene materials, Nano Lett. **10**, 1125 (2010).

[55] J. Bai, X. Zhong, S. Jiang, Y. Huang, and X. Duan, Graphene nanomesh, Nat. Nanotechnol. **5**, 190 (2010).

[56] M. Kim, N. S. Safron, E. Han, M. S. Arnold, and P. Gopalan, Electronic transport and Raman scattering in size-controlled nanoperforated graphene, ACS Nano **6**, 9846 (2012).

[57] M. Begliarbekov, O. Sul, J. Santanello, N. Ai, X. Zhang, E.-H. Yang, and S. Strauf, Localized states and resultant band bending in graphene antidot superlattices, Nano Lett. **11**, 1254 (2011).

[58] Q. Xu, M.-Y. Wu, G. F. Schneider, L. Houben, S. K. Malladi, C. Dekker, E. Yucelen, R. E. Dunin-Borkowski, and H. W. Zandbergen, Controllable atomic scale patterning of freestanding monolayer graphene at elevated temperature, ACS Nano **7**, 1566 (2013).

[59] F. Oberhuber, S. Blien, S. Heydrich, F. Yaghobian, T. Korn, C. Schuller, C. Strunk, D. Weiss, and J. Eroms, Weak localization and Raman study of anisotropically etched graphene antidots, Appl. Phys. Lett. **103**, 143111 (2013).